Graphene rotational switch through vacancy defect and nitrogen doping

Mohammad Poliki, Mozhgan Golzani, Saeed Haji-Nasiri ✉

Faculty of Electrical, Biomedical and Mechatronics Engineering, Qazvin Branch, Islamic Azad University, Qazvin, Iran
✉ *E-mail: s.nasiri@qiau.ac.ir*

Published in Micro & Nano Letters; Received on 13th June 2019; Revised on 13th April 2020; Accepted on 27th April 2020

A graphene rotational switch (GRS) is presented utilising vacancy defect and nitrogen (N) doping in armchair graphene nanoribbon (AGNR). By twisting AGNR at different angles in the suggested device, its conductivity can be controlled. Based on the simulation results it is indicated that the electronic parameters such as current, transmission, local density of state, and conductance of the suggested GRS are also associated with the width of AGNR, selection of defect or doping and its location in the AGNR. Furthermore, the results show the dependency of the proposed GRS to the voltage. In this Letter, a monotonic increase or decrease in the current between the minimum and maximum angles in the corresponding bias voltage is defined as the proper switching behaviour. The assumed defect or doping is replaced by three locations with three various widths and five different twist angles of AGNR, in different analysed modes. Devices have better switching behaviour so the range of I_{max}/I_{min} is within 37–1076 among all the modes. The best three modes are the perfects, N doping near the AGNR edge and the vacancy defect in the centre of the deformation region of AGNR in the width of 9, 10 and 11w, respectively.

1. Introduction: Graphene is a proper candidate for using in nanoscale electronic devices as a result of extraordinary properties such as high mobility, flexibility, extreme thermal and electrical conductivity and surprising mechanical strength [1, 2]. Various band gaps can be obtained depending on the type of ribbon edge by converting graphene into graphene nanoribbon (GNR) [3]. To control the GNR deformation as the twist is considered a suitable method to modify its electrical properties [4–6]. In the twist study, the superior impact of the twist on the edge of the armchair GNR (AGNR) compared to the edge of zigzag GNR directs the AGNR usage [7]. The twist in the GNR is obtained via carbon nanotubes [8], chemical etching [9, 10], epitaxy [5], chemistry at the edges of saturated GNRs [11, 12] or tilt grain boundaries [13]. Applying an external magnetic field to the electrodes [7, 14] or to one electrode (keeping the other electrode constant) [15–17] also causes twist. The twisted GNRs on a soft substrate were found, which posed a challenge to prevent GNRs from bubble and buckle on the substrate [18]. Moreover, in most devices, GNRs are twisted with no substrate [13].

2. Materials and methods: The nanoribbon width and the applied defects can also be considered as the parameters in addition to the twist to the electronic properties of AGNR more accurately [6]. AGNRs are divided into three groups, which include a medium-gap ($3p$), large-gap ($3p+1$) and very small-gap ($3p+2$) nanoribbon, each of which has different electronic properties [3]. Three widths of AGNR with 9, 10 and 11 atoms (9, 10, 11w) with a fixed length are chosen. Fig. 1 represents the typical structure of the proposed device, in this study. Based on Fig. 1*a*, three different parts compromise the device: the right electrode (RE), the left electrode (LE) and the scattering region (SR). The SR has two sections consisting of a deformation region under twist and two flat interval regions near the left and REs with no twist. The twisted AGNRs are composed of semi-infinite right and LEs separated by the SR, that the deformation region is in contact with two flat interval regions essential for the electrostatic potential at the edge of the SR to converge to the value of the electrodes, and semi-infinite electrodes remain with no twist [6]. The suggested device shown in Fig. 1*a* is in the perfect mode (without defect) with a twist angle of 60° and width of 10w. The LE in the supposed twist is fixed and the RE is twisted in the direction of the x-axis. The locations of N doping on the edge and the centre of right flat interval and the centre of deformation region, are represented by NE, NF and NC, respectively. Moreover, VE, VF and VC show the vacancy defects in the same three locations.

During N doping to AGNR, three configurations including pyridinic N, pyrrolic N and graphitic N (quaternary N) are possible. Among these, two configurations of pyridinic N and graphitic N have sp^2 hybridisation and pyrrolic N has sp^3 hybridisation. In pyridinic N type doping, a nitrogen atom bonds to two carbon atoms at the edges of a GNR and an electron from the orbital p enters the π system. Moreover, in the graphitic N type doping, nitrogen atom replaces instead of the carbon atom in the hexagonal ring [19, 20]. Therefore, in all three widths of NE, the doped nitrogen is pyridinic N type and for NC and NF modes, the doped nitrogen is graphitic N type. In widths of 9, 10 and 11w, the ratio of nitrogen to the total structure is 0.55, 0.5 and 0.45%, respectively.

Fig. 1*b* indicates the twist for five different angles at room temperature while considering fully relaxation for the atomic structure. Moreover, due to the clarity of changes in the electronic transmission characteristics during the twist process, an acceptable range of angles is studied, the number of outputs is controlled, and the twist angles were chosen 60°. This structure is initially offered as a graphene rotational switch (GRS).

Nowadays, the reduction of devices and the demand for low consumption of power in of nano electromechanical systems (NEMS) have been considered. Graphene with high young's modulus and as well as higher elasticity than other materials is used in NEMS [21]. Therefore, the production of low pull-in voltage graphene-based NEMS switches can be applicable. NEMS switches are recommended for low power consumption, high on-off ratio, and reduction of leakage current in devices, and are also used in logic circuits, data storage and high frequency communication [22]. There are two ways to make NEMS switches: in one mode both ends of the structure are fixed and in the other mode one end of the structure is fixed and the other side is movable [23, 24] such that this method has been used in this study to make the switch. In the current study, this method has been used to make the proposed GRS.

The used calculation method in the suggested GRS is a combination of density functional theory technique and non-equilibrium Green's function [25].

Also the generalised gradient approximation is employed for exchange-correlation potential. The Atomistix ToolKit (ATK-2016.4) package is used for calculations and the optimisation

© The Institution of Engineering and Technology 2020

doi: 10.1049/mnl.2019.0377

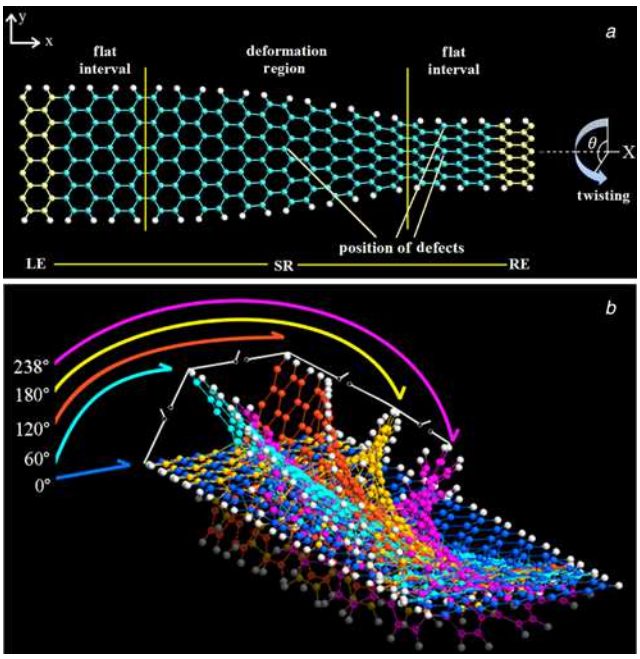


Fig. 1 *Typical structure of the suggested device* a *under* *a* twist angle of 60° in the width of 10w and three locations of the defects, *b* AGNR (SR of the suggested device) with the width of 10w under five various twist angles (θ = 0, 60, 120, 180, 238°)

process [26]. The k-points mesh of $1 \times 1 \times 100$ within the Monkhorst-Pack scheme is used to sample the Brillouin zone of the electrodes and the cut off energy is set to 150 Ry.

We use the following equation to calculate the transfer function ($T(E, V)$), E and V are energy and voltage of the device, respectively [27]

$$T(E, V) = \text{Trace}[\Gamma_L G^D \Gamma_R G^A] \tag{1}$$

where $G^{D(A)}$ is the delayed (advanced) Green's function of the SR and $\Gamma_{L(R)}$ is a factor associated with the broadening of the left (right) electrode that is equal [27]

$$\Gamma_{L(R)} = i\left[\sum\nolimits_{L(R)} - \sum\nolimits^{\dagger}_{L(R)}\right]\left(\frac{\pi}{2} - \theta\right) \tag{2}$$

$\Sigma_{L(R)}$ is the left (right) electrode self-energy function explaining the shift and broadening of the energy levels because of the interaction with the left (right) electrode. Furthermore, using the following equation the current (I) is determined [27]

$$I(V) = \frac{2e}{h}\int_{\mu_L}^{\mu_R} T(E, V)\left[f(E, \mu_L) - f(E, \mu_R)\right] \mathrm{d}E \tag{3}$$

where e and h are the charge of the electron and Planck's constant, respectively, $T(E, V)$ the transmission function of the device, μ_L and μ_R represent the chemical potentials of the left and REs, respectively, and $f(E, \mu)$ shows the Fermi–Dirac distributions.

One of the most important issues in electronic transmission is the conductance. It can be said that in the nanoscale dimensions, the conductance is a function of the bias voltage. The conductance is defined by the following equation that $T(E_F)$ is the transmission coefficient in Fermi energy and G_0 is the quantum conductance [27]:

$$G = T(E_F)G_0, \quad G_0 = \frac{2e^2}{h} \tag{4}$$

Moreover, the amount of conductance in devices can be expressed as a function of left (T_L) and right (T_R) electrodes by the transmission spectrum. In semiconductors, conductance is often determined by the distribution of hot electrons or holes with conductance band or valence band that is called thermionic emission. Hot electrons are located in the energy range along the Fermi function. It can be said that in $T_L = T_R = 0$, the conductance is determined by the transfer coefficient at the Fermi level. Moreover, when the temperature is given to the electrode, the conductance will depend on the value of the transfer coefficient in the energy range around the Fermi level and is calculated using the following equation, where K_b is the constant of Boltzmann and f' is the derivative of the Fermi function [28]:

$$\sigma(T_L) = \frac{2e^2}{h}\int T(E) f'\left(\frac{E - E_F^L}{k_b T_R}\right)\frac{\mathrm{d}E}{k_b T_R} \tag{5}$$

3. Results: The twist relies on the width of the ribbon and an increase in the twist angle changes the strain energy of the structure [6, 29]. The last angle before the breakdown of the AGNR carbon bonds is known as the critical angle. The critical angle is oppositely related to the width of AGNR. Furthermore, the critical angle is altered either by defect or doping and by the location of the doping or defect. Appropriate switching behaviours are found in GRS-9w-NF, GRS-10w-NE, and GRS-11w-NE for N doping and in GRS-9w-VE, GRS-10w-VF, and GRS-11w-VC for vacancy defect. Among all the above modes, the most proper switching behaviour is found for GRS-9w-NF, GRS-10w-NE and GRS-11w-VC with the bias voltages of 2, 1.3 and 0.2 V, respectively. The best switching behaviour in the perfect mode is seen in the GRS-9w and GRS-10w. Moreover, in the width of 11w in the perfect mode, no switching behaviour is found since by increasing twist angle up to 60° the current is increased, then, it is decreased by incrementing the angle to the critical angle. Nevertheless, this alternation trend in the GRS-11w-NE is within the bias of 0–2 V and GRS-11w-VC is only at 0.2 V. Therefore, by employing the twist the current reduces. By retaining the doping at the width of 10w, better switching behaviour is observed compared to the perfect mode, however, the best switching behaviour in the width of 9w can be observed in the perfect mode. Additionally, by applying doping, the width of 10w involves a higher I_{max}/I_{min} compared to the width of 11w.

4. Discussion: According to the results obtained, we investigate the electronic transport properties of GRS-10w. As an instance Fig. 2 represents the current, transmission spectra and local density of state (LDOS) in subfigures *a*–*c*, respectively, for the suggested device under the bias voltage of 1.3 V for GRS-10w-NE. The nanoribbon is located under the angles of 0, 60, 120, 180° with the critical angle of 240°. With increasing twist angle in all the modes in the width of 10w, the passing current is also increased that is shown in GRS-10w-NE. According to Fig. 2*b*, this incremental trend is well demonstrated in the transmission curve in GRS-10w-NE with an increment in the area under the curve. In addition, the shape of LDOS for the non-twisting (0°) and the critical angle was plotted for the minimum and maximum electron density distribution at a Fermi level of 0.18 eV, respectively. The LDOS can show us information about the distribution of electron channels at a specific energy level of the device in real space.

The highest density dispersion of the state is associated with the highest twist angle, indicating that the maximum current passes through the device. However, with increasing twist angle in all the modes for the width of 9w, the passing current is reduced.

Fig. 3, shows the current–voltage column graph for 10w modes with the most encouraging switching behaviour in the bias

© The Institution of Engineering and Technology 2020

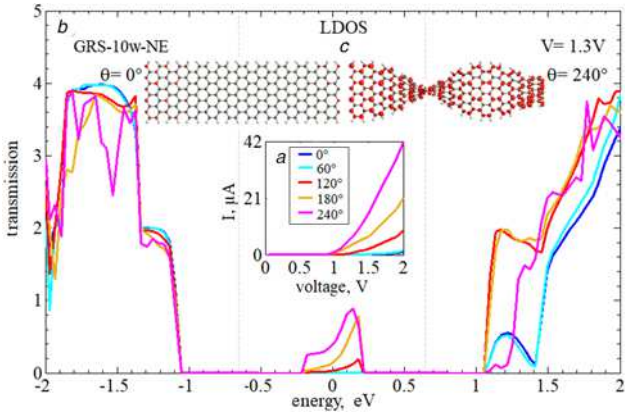


Fig. 2 *The electronic transport features in GRS-10w-NE*
a Current,
b Transmission spectra,
c LDOS under the bias voltage of 1.3 V at 0.18 eV energy

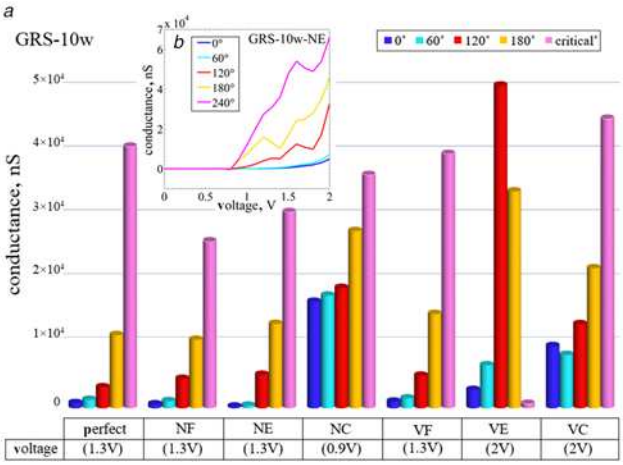


Fig. 4 *The conductance–voltage*
a column graph for all modes of 10w under various bias voltages in different angles
b curve for GRS-10w-NE in different angles (each colour represents an angle)

voltage of 1.3 V for the perfect, NE, NF and VF modes and the bias voltage of 0.9 V for the NC mode. In these modes, with increasing twist angle, there is a monotonic behaviour for the current thereby the highest I_{max}/I_{min}. The optimal switching behaviour in this article is explained as a monotonic increase or decrease in the current between the minimum (0°) and maximum (critical) angles in the corresponding bias voltage. In additions, the current–voltage diagram for VC and VE modes are indicated in this Figure as well, to show an adverse switching behaviour. According to the VC and VE modes illustrated with hachure colours, by increasing twist angle there was no monotonic behaviour in the current.

In Fig. 4, the column graph of conductance versus voltage is plotted under different twist angles for all modes at 10w width in the bias where it showed the most appropriate switching behavior. In this width, the conductance increases with increasing twist angle for all modes except VE and VC modes. In Fig. 3, the monotonic behavior of these two modes did not have increasing trend as the twist angle increased that led to a lack of switching behavior. In the conductance graphs of these two modes, this is clearly seen that they behave in a non-monotonic manner by changing the twist angle. To better understand this issue, the conductance–voltage curve for the GRS-10w-NE mode has been plotted at 0–2 V at different twist angles (Fig. 4*b*), and an increase in conductance is observed as the voltage increases. Moreover, the twist angle has a significant effect on the conductance in the same bias. In fact, the twist leads to the strain in the structure changing the bandgap and thus the conductivity of AGNR [30].

Just as voltage changes the conductivity, similarly the temperature affects the conductivity. For example, the effect of temperature on conductance for the GRS-10w-NE and GRS-9w-perfect modes under different twist angles has been shown in Figs. 5*a* and *b*, respectively. At low temperatures, by changing the twist angle from 0° to 240°, the monotonic increase in conductance is clearly seen, but this condition is not established for higher temperatures ($T > 300$). For example, at 373K (100°C), the conductance has been increased by an average of 30.83 times for all angles temperature comparing to 300 K. Therefore, although different twist angles have different conductance under different temperatures, but in general, temperature has a great effect on conductance for all modes, and conductance has increased with increasing temperature. In the GRS-9w-perfect mode like the GRS-10w-NE mode, the conductance increases with increasing temperature, expect that in this width (9w), conductance will be less with increasing the twist angle.

The maximum and minimum passing currents in the corresponding angles for 9, 10 and 11w widths at the chosen bias voltage are provided in Table 1. In all of the widths, at the determined angle, the bias voltages are chosen so that for the minimum electronic conductivity I_{min} is close to zero. These currents are selected to indicate the most appropriate switching modes. Table 1 shows the effect of selecting the defect or doping and its location in the determined width on I_{max} and I_{min} of the switch.

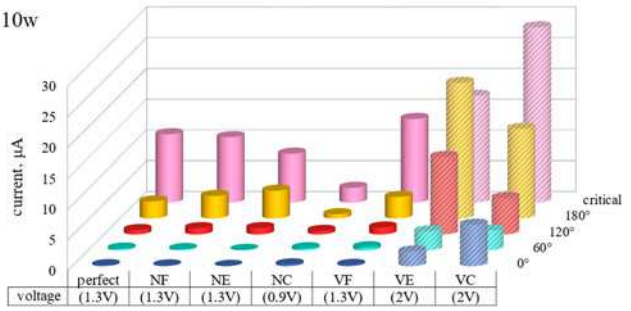


Fig. 3 *Current–voltage column graph for all modes of 10w under various bias voltages in different angles (each colour represents an angle)*

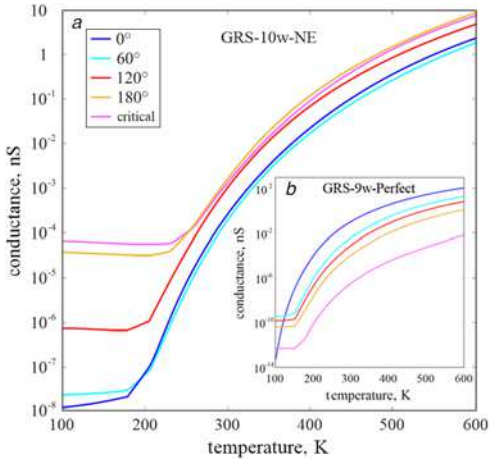


Fig. 5 *Conductance versus different temperatures in*
a GRS-10w-NE mode,
b GRS-9w-perfect mode

© The Institution of Engineering and Technology 2020

doi: 10.1049/mnl.2019.0377

Table 1 Maximum and minimum current of the devices along with their associated angles under various bias voltages for all the modes

Mode	Location	Perfect	NC	NE	NF	VC	VE	VF
9 w	voltage	2, V	1.3, V	2, V	2, V	1.8, V	2, V	2, V
	degree, $\theta°$	0°	0°	0°	0°	0°	0°	0°
	I_{max}, μA	17.22	11.71	3.65	5.28	6.29	11.19	5.04
	degree, $\theta°$	285°	285°	285°	288°	273°	260°	285°
	I_{min}, μA	0.01	0.57	0.08	0.01	0.25	0.31	0.02
	voltage	1.3, V	0.9, V	1.3, V	1.3, V	2, V	2, V	1.3, V
10w	degree, $\theta°$	238°	238°	240°	238°	225°	241°	238°
	I_{max}, μA	11.03	2.41	7.86	10.56	28.47	17.31	13.54
	degree, $\theta°$	0°	0°	0°	0°	0°	0°	0°
	I_{min}, μA	0.15	0.28	0.03	0.11	6.74	2.38	0.19
	voltage	0.2, V	0.2, V	0.2, V	0.2, V	0.2, V	0.2, V	0.2, V
11w	degree, $\theta°$	0°	0°	0°	0°	0°	0°	0°
	I_{max}, μA	13.46	14.09	14.36	13.48	13.73	12.79	13.53
	degree, $\theta°$	212°	213°	212°	212°	201°	186°	217°
	I_{min}, μA	0.16	5.82	0.18	0.32	0.15	0.03	0.12

5. Conclusion: Defect or doping in twisted AGNR aims to make promising switching behaviour. Any variations in the current and critical angle rely on the AGNR width, choosing the defect or doping and its location on the AGNR. In the width of 9w, switching behaviour can be observed for all the modes except for the VF mode. However, in the perfect mode, GRS-9w-NF, and GRS-9w-VE, respectively, the best switching behaviour can be obtained. Good switching behaviour is observed in the width of 10w, for the perfect mode related to the GRS-10w-VF. While considering GRS-10w-NE, a better switching behaviour exists compared to both modes. In the width of 11w, by changing the twist angle, there was no monotonic behaviour in the current. Nevertheless, using the VC and NE, a monotonic and optimal switching behaviour exists for the bias voltages of 0.2 and 0–2 V, respectively. The results indicate that in AGNRs, through changing the electro-mechanics, the electronic properties can be adjusted, hence, it can be utilised as an appropriate switch in the new NEMS.

6 References

[1] Peres N.M.R., Guinea F., Neto A.C.: 'Electronic properties of disordered two-dimensional carbon', *Phys. Rev. B.*, 2006, **73**, (2), p. 125411

[2] Novoselov K.S., Geim A.K., Morozov S.V., *ET AL.*: 'Electric field effect in atomically thin carbon films', *Science*, 2004, **306**, (5696), pp. 666–669

[3] Son Y.W., Cohen M.L., Louie S.G.: 'Energy gaps in graphene nanoribbons', *Phys. Rev. Lett.*, 2007, **98**, (8), p. 089901

[4] Gui G., Morgan D., Booske J., *ET AL.*: 'Local strain effect on the band gap engineering of graphene by a first-principles study', *Appl. Phys. Lett.*, 2015, **106**, (5), p. 053113

[5] Park J., Mitchel W.C., Elhamri S., *ET AL.*: 'Observation of the intrinsic bandgap behaviour in as-grown epitaxial twisted graphene', *Nat. Commun.*, 2015, **6**, p. 5677

[6] Jia J., Shi D., Feng X., *ET AL.*: 'Electromechanical properties of armchair graphene nanoribbons under local torsion', *Carbon. NY*, 2014, **76**, pp. 54–63

[7] Li H., Al-Aqtash N., Wang L., *ET AL.*: 'Electromechanical switch in metallic graphene nanoribbons via twisting', *Physica E*, 2012, **44**, (10), pp. 2021–2026

[8] Chamberlain T.W., Biskupek J., Rance G.A., *ET AL.*: 'Size, structure, and helical twist of graphene nanoribbons controlled by confinement in carbon nanotubes', *ACS Nano*, 2012, **6**, (5), pp. 3943–3953

[9] Elias A.L., Botello-Mendez A.R., Meneses, *ET AL.*: 'Longitudinal cutting of pure and doped carbon nanotubes to form graphitic nanoribbons using metal clusters as nanoscalpels', *Nano Lett.*, 2009, **10**, (2), pp. 366–372

[10] Antidormi A., Royo M., Rurali R.: 'Electron and phonon transport in twisted graphene nanoribbons' *J. Phys. D.*, 2017, **50**, (23), p. 234005

[11] Gunlycke D., Li J., Mintmire J.X., *ET AL.*: 'Edges bring new dimensions to graphene nanoribbons', *Nano Lett..*, 2010, **10**, (9), pp. 3638–3642

[12] Nikiforov I., Hourahine B., Frauenheim T., *ET AL.*: 'Formation of helices in graphene nanoribbons under torsion' J. *Phys. Chem. Lett.*, 2014, **5**, (23), pp. 4083–4087

[13] Liu X., Wang F., Wu H.: 'Anomalous twisting strength of tilt grain boundaries in armchair graphene nanoribbons', *Phys. Chem. Chem. Phys.*, 2015, **17**, (47), pp. 31911–31916

[14] Al-Aqtash N., Li H., Wang L., *ET AL.*: 'Electromechanical switching in graphene nanoribbons', *Carbon. NY*, 2013, **51**, pp. 102–109

[15] Xia D., Li Q., Xue Q., *ET AL.*: 'Super flexibility and stability of graphene nanoribbons under severe twist', *Phys. Chem. Chem. Phys*, 2016, **18**, (27), pp. 18406–18413

[16] Li Y.: 'Twist-enhanced stretchability of graphene nanoribbons: a molecular dynamics study' *J. Phys. D*, 2010, **43**, (49), p. 495405

[17] Cranford S., Buehler M.J.: 'Twisted and coiled ultralong multilayer graphene ribbons', *Model. Simul. Mater. Sci. Eng*, 2011, **19**, (5), p. 054003

[18] Zhang D.B., Seifert G., Chang K.: 'Strain-induced pseudomagnetic fields in twisted graphene nanoribbons', *Phys. Rev. Lett.*, 2014, **112**, (9), p. 096805

[19] Senturk A.K., Oktem A.S., Konukman A.E.S.: 'Influence of defect locations and nitrogen doping configurations on the mechanical properties of armchair graphene nanoribbons' *J. Mol. Model.*, 2018, **24**, (2), p. 43

[20] Wang H., Maiyalagan T., Wang X.: 'Review on recent progress in nitrogen-doped graphene: synthesis, characterization, and its potential applications', *ACS Catal.*, 2012, **2**, (5), pp. 781–794

[21] Kang J.W., Kim H.W., Kim K.S., *ET AL.*: 'Molecular dynamics modeling and simulation of a graphene-based nanoelectromechanical resonator', *Curr. Appl. Phys.*, 2013, **13**, (4), pp. 789–794

[22] Sun J., Wang W., Muruganathan M., *ET AL.*: 'Low pull-in voltage graphene electromechanical switch fabricated with a polymer sacrificial-spacer', *Appl. Phys. Lett*, 2014, **105**, (3), p. 033103

[23] Zulkefli M.A., Mohamed M.A., Siow K.S., *ET AL.*: 'Optimization of beam length and air gap of suspended graphene NEMS switch for low pull-in voltage application'. 2016 IEEE Int. Conf. on Semiconductor Electronics (ICSE), Kuala Lumpur, Malaysia, August 2016, pp. 29–32

[24] Zulkefli M.A., Mohamed M.A., Siow K.S., *ET AL.*: 'Three-dimensional finite element method simulation of perforated graphene nano-electro-mechanical (NEM) switches', *Micromachines. (Basel)*, 2017, **8**, (8), p. 236

[25] Ning Z.: 'First principles quantitative modeling of molecular devices'. PhD Dissertation, McGill University Library, 2010

[26] 'Atomistix ToolKit version 2016.4, QuantumWise A/S' Available at http://www.quantumwise.com

[27] Datta S.: 'Quantum transport: atom to transistor' (Cambridge University Press, Cambridge, 2005)

[28] Masoumi S., Hajghasem H., Erfanian A., *ET AL.*: 'Simulation field effect transistor bipolar graphene nano-ribbon', *Proc. Mater. Sci.*, 2015, **11**, pp. 407–411

[29] Sadrzadeh A., Hua M., Yakobson B.I.: 'Electronic properties of twisted armchair graphene nanoribbons', *Appl. Phys. Lett.*, 2011, **99**, (1), p. 013102

[30] Dobrinsky A., Sadrzadeh A., Yakobson B.I., *ET AL.*: 'Electronic structure of graphene nanoribbons subjected to twist and nonuniform strain', *Int. J. High Speed Electron. Syst.*, 2011, **20**, (1) pp. 153–160

© The Institution of Engineering and Technology 2020